Macromolecules

Article

pubs.acs.org/Macromolecules

Direct Measurements of Polymer Brush Conformation Using Small-Angle Neutron Scattering (SANS) from Highly Grafted Iron Oxide Nanoparticles in Homopolymer Melts

Michael J. A. Hore,[†,*] Jamie Ford,[‡] Kohji Ohno,[⊥] Russell J. Composto,[§,∥] and Boualem Hammouda[†]

[†]Center for Neutron Research, National Institute of Standards and Technology, 100 Bureau Drive, Gaithersburg, MD 20899, United States

[‡]Penn Regional Nanotechnology Facility, University of Pennsylvania, Philadelphia, Pennsylvania 19104, United States

[⊥]Institute for Chemical Research, Kyoto University, Uji, Kyoto 611-0011, Japan

[§]Department of Materials Science & Engineering, University of Pennsylvania, Philadelphia, Pennsylvania 19104, United States

[∥]Laboratory for Research on the Structure of Matter (LRSM), 3231 Walnut Street, Philadelphia, Pennsylvania 19104, United States

ABSTRACT: Small-angle neutron scattering (SANS) is a sensitive technique that is able to probe the structure of polymer-grafted nanoparticles and free polymer chains. Here, we combine SANS measurements with self-consistent field theory (SCFT) calculations to study the structure of deuterated poly(methyl methacrylate) (dPMMA) nanocomposites containing PMMA-grafted Fe_3O_4 nanospheres, with a specific emphasis on the conformation of the PMMA brush chains. We present a new, detailed SANS model which is able to account for the excluded volume of the grafted polymer chains, and compare the experimentally measured brush chain conformations to predictions from SCFT calculations for a polymer-grafted nanosphere, and previous studies by others. The results of the SANS measurements are in qualitative agreement with SCFT calculations and in excellent quantitative agreement with previous studies that indirectly assessed the structure of the polymer chains by measuring the hydrodynamic radius of the nanoparticles. Unlike previous methods, however, SANS provides direct measurements of the polymer brush conformation.

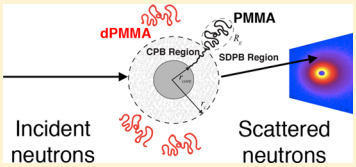

INTRODUCTION

Nanoparticles are added to polymer materials to enhance properties such as optical absorption, Raman scattering, or electron transport. Their utility in these applications, however, is determined largely by their distribution within the polymer matrix. For instance, uniform dispersion and vertical orientation of CdSe nanorods is key to enhancing electron transport in thin film polymer photovoltaic devices.[1] Because of the prevalence of polymer nanocomposites in a variety of products and technologies, a large amount of research effort is dedicated to understanding fundamental topics related to their fabrication, processing, and structure−property relationships.

A key issue related to the fabrication and processing of polymer nanocomposites is the morphology of nanoparticles within the material. Specifically, under what conditions do the nanoparticles disperse or aggregate in the material? To incorporate nanoparticles into a polymer, a polymer brush is often grafted to the particle surface, which in turn makes the particles compatible with the polymer matrix. In the athermal case, where the brush and matrix are chemically similar and the Flory−Huggins parameter $\chi \approx 0$, nanoparticle dispersion is primarily characterized by the ratio of length (i.e., degree of polymerization) of the matrix chains (P) to that of the brush chains (N), $\alpha = P/N$. The values of α that dictate nanoparticle dispersion or aggregation have received considerable attention in recent years, and additional details can be found in the recent reviews from Green[2] and Kumar et al.[3] for polymer-grafted nanospheres, and in the work of Hore, Frischknecht, and Composto for the case of gold nanorods.[4−6] Jiao and Akcora[7] recently demonstrated that for polymer-grafted Fe_3O_4 nanospheres, a combination of autophobic dewetting and magnetic interactions leads to further control over the aggregation of nanoparticles in polymer nanocomposites.

In addition to the influence of brush chain conformation on nanoparticle dispersion, the conformation of brush chains is an important characteristic for predicting the diffusion of polymers within a nanocomposite. Recently, work by Gam et al.[8,9] and Choi et al.[10] has demonstrated that polymer diffusion coefficients in nanocomposites can be collapsed onto a master curve using the confinement variable $ID/2R_g$, where ID is the average interparticle separation in the composite and R_g is the radius of gyration of the diffusion tracer polymer. For nanoparticles that have a dense brush of high molecular weight polymer on their surface, Choi et al. showed that the diffusion of a tracer within the nanocomposite network is dependent upon the degree to which the tracer can penetrate the brush. Thus, ID depends not only on nanoparticle volume fraction, but also on the conformation of chains within the brush. *A priori*, one might also expect the shape of the nanoparticle to influence ID because of changes in particle−particle separation

Received: September 24, 2013
Revised: October 31, 2013
Published: November 21, 2013

distances as well as changes in the conformation of the polymer brush chains when grafted to surfaces of various curvatures.

In the work of Alexander[11] and de Gennes,[12] a polymer chain grafted to a planar substrate adopts a non-Gaussian conformation due to crowding effects from its neighbors, leading to a brush thickness that scales as $h \sim N$. Daoud and Cotton[13] extended the Alexander-de Gennes brush model to the case of star polymers, where all chains are spherically symmetric about a central grafting point. The crowding of neighboring chains plays a slightly diminished role in this case, leading to a weaker scaling with N than in the planar case. This model has since been extended to describe polymer chains grafted onto curved, convex surfaces[14,17,18] and calculations of brushes grafted onto convex surfaces have also been performed using SCFT.[21−24] Laradji performed Monte Carlo simulations of polymers grafted onto curved, fluctuating surfaces, which has relevance for biomaterials applications.[15,16] Recent work from Ohno et al.[17] and Dukes et al.[18] has specifically focused on the structure of polymer chains grafted to spherical nanoparticles at high grafting densities using dynamic light scattering (DLS) measurements in solution to study the brush height, h. The findings of both Ohno et al. as well as Dukes et al. show two primary regions of the brush. Near the nanoparticle surface, up to a crossover radius r_c, the brush is said to be a concentrated polymer brush (CPB). Monomers in the CPB regime are highly crowded, leading to a high degree of stretching in each brush chain. Here, both Ohno et al.[17] and Dukes et al.,[18] measured $h \sim n^{4/5}$ in the CPB region, where n is the number of polymer segments within the CPB region. Linear scaling is only expected for dimensionless grafting densities $\sigma^* = a^2\sigma \rightarrow 1$, thus a smaller scaling exponent was observed (a is the statistical segment length). Near r_c, the brush transitions from the CPB region to a semidilute polymer brush (SDPB) region, in which the height scales as $h \sim m^{3/5}$ for a degree of polymerization $n < m \leq N$ in a good solvent. Monomers in the SDPB regime of the brush are less crowded, and can adopt a more ideal conformation. By extending the Daoud−Cotton model, Ohno et al. obtain the critical radius as

$$r_c = r_{core}\sigma^{*1/2}\nu^{*-1} \quad (1)$$

where $\nu^* = \nu/(4\pi)^{1/2}$, and ν is the excluded volume parameter for the polymer chain. Note that r_c is the distance from the *center* of the nanoparticle to the SDPB region, thus the thickness of the CPB region is $r_{shell} = r_c - r_{core}$. The CPB and SDPB regimes of a highly grafted nanoparticle are shown schematically in Figure 1. Note that if $r_{core} > r_c$, the entire brush is in a SDPB region, and no CPB region exists. More recently, work from the Bockstaller group[19,20] examined the scaling of the SDPB and CPB regions of densely grafted SiO_2 nanoparticles in polymer melts. From analysis of transmission electron microscopy images, Choi et al.[19,20] determined the size of the CPB region scales as $h \sim n^{0.8}$, whereas in a polymer melt, the SDPB region scales as $h \sim m^{0.5}$, indicating that the regions of the brush chains within the SDPB behave as ideal chains. This is in contrast to the results of Ohno[17] and Dukes et al.[18] which demonstrated the SDPB region behaves as a swollen coil in a good solvent. Note that in all three of these previous studies, the scaling of the SDPB and CPB regions was determined indirectly through either image analysis or light scattering. In this work, small-angle neutron scattering (SANS) is used to directly measure these length scales for the first time in a polymer melt.

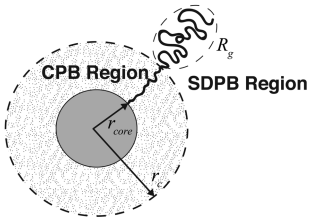

Figure 1. Schematic representation of a highly grafted nanoparticle with the concentrated polymer brush (CPB) and semidilute polymer brush (SDPB) regions. r_{core} is the radius of the nanoparticle, and r_c is the cutoff distance that separates the CPB and SDPB regions. R_g is the radius of gyration of the portion of the chain that resides in the SDPB region.

To date, only a handful of studies have used SANS to measure polymers grafted to nanoparticles. Chevigny et al.[25−27] performed both SANS and small-angle X-ray scattering (SAXS) measurements on polystyrene-grafted silica particles in solution and in a homopolymer melt. A key finding was that a core−shell model is not sufficient to accurately model the scattering from the nanoparticles used in the study, and a model that accounts for the grafted chain conformation is needed.[25] The silica particles used in this study had a polystyrene grafting density of $\sigma = 0.2$ chains/nm^2 and a molecular weight of M_n = 25 000 g/mol. The SANS intensities were fit using a model developed by Pedersen to describe scattering from block copolymer micelles.[28] This model assumes a spherical core that is grafted with ideal, Gaussian chains, and can be extended to nonspherical cores.[29] Recently, Vogiatzis and Theodorou[30] performed extensive Monte Carlo simulations of polystyrene-grafted silica nanoparticles in a polystyrene matrix, and compared the results to the neutron scattering experiments of Chevigny et al.[26] The Monte Carlo results agree well with the SANS measurements. Interestingly, the authors note that the brush thickness, determined from the simulations, depends only upon the grafting density and brush chain molecular weight. Hence, no substantial difference in the brush density profile was observed between high and low molecular weight matrices. This result is in good agreement with recent SCFT and DFT results.[5] Recent work has also used SANS to characterize polystyrene-grafted γ-Fe_2O_3 nanoparticles using a Gaussian-chain model.[31,32]

In this paper, spherical, PMMA-grafted iron oxide (Fe_3O_4) nanoparticles (radius r_{core} = 2.5 nm) are investigated. Because the PMMA is attached to the nanoparticle surface using atom-transfer radical polymerization (ATRP), a grafting-from approach, the grafting density is highly uniform as a function of brush molecular weight. Hence, this system is an ideal model for studying brush chain conformation on a highly grafted, highly curved surface, since the grafting density is precisely controlled. SANS is performed for brushes having molecular weights of 4, 9, 13, 27, and 36 kg/mol at a fixed grafting density of $\sigma = 0.73$ chains/nm^2, corresponding to approximately 60 chains per nanoparticle. Using eq 1, r_c for these PMMA-grafted iron oxide nanoparticles is estimated to be between 5.6 and 7.0 nm. To augment the SANS measurements, self-consistent field theory (SCFT) calculations are performed to determine the conformation and excluded volume parameter for an individual brush chain grafted to a nanoparticle. Finally, we present a detailed SANS model that does not assume that the grafted PMMA chains are Gaussian, and which is an appropriate description for scattering from polymer-grafted nanoparticles in

dx.doi.org/10.1021/ma401975a | *Macromolecules* 2013, 46, 9341−9348

non-Θ solvents, in homopolymer melts with specific interactions, or for stretched polymer chains.

THEORETICAL METHODS

SCFT of Polymer-Grafted Nanoparticles. Self-consistent field theory (SCFT) is a mean field, statistical path integral framework that has been successful in calculating many important quantities for polymeric systems. For example, the phase diagram for block copolymer melts, the interaction between polymer-grafted nanoparticles in homopolymer melts, and the structure of polymer brushes in miscible polymer blends have all been well-described by SCFT.[5,21−23,33,34,36] The partition function for a system of a single polymer-grafted nanoparticle embedded in a chemically identical homopolymer melt, containing n_b brush chains and n_m matrix chains is given by

$$\mathcal{Z} = \int \prod_{i=1}^{n_b} \mathcal{D}\mathbf{R}_{b,i}(s) \int \prod_{j=1}^{n_m} \mathcal{D}\mathbf{R}_{m,j}(s) \exp(-\beta U_0[\mathbf{R}_{b,i}(s)] - \beta U_0[\mathbf{R}_{m,j}(s)]) \times \delta[1 - \hat{\phi}_b - \hat{\phi}_m - \hat{\phi}_{NP}] \quad (2)$$

The potential U_0 corresponds to a harmonic potential between monomers, and for an arbitrary chain m is taken to be

$$U_0[R_{l,m}(s)] = \frac{3}{2a^2} \int_0^{N_l} \mathrm{d}s \left| \frac{\partial R_{l,m}(s)}{\partial s} \right|^2 \quad (3)$$

where a is the statistical segment length and N_l is the degree of polymerization of a chain of type l. The brush chains are grafted to the nanoparticle surface at a reduced grafting density

$$\sigma^* = \frac{\sigma\sqrt{6N}}{a\rho_0} \quad (4)$$

where $1/\rho_0$ is the volume of a single monomer. For hydrogenated PMMA, $1/\rho_0 \approx 0.158$ nm^3.

Equation 2 is transformed into a partition function described by an auxiliary field $\omega_+(\mathbf{r})$ through integral transformations into a form

$$\mathcal{Z} = \int \mathcal{D}\omega_+ \exp(-\mathcal{H}[\omega_+]) \quad (5)$$

with the effective Hamiltonian $\mathcal{H}$ expressed as

$$\frac{\mathcal{H}}{k_B T C} = -\frac{1}{V} \int i\omega_+(r)\, \mathrm{d}\mathbf{r} - \phi_b \ln Q_b - \phi_m \alpha^{-1} \ln Q_m \quad (6)$$

where $C = \rho_0 V/N$. Q_b and Q_m are the single chain partition functions of the brush and matrix, respectively.

A mean field approximation is imposed, leading to the common "self-consistent field theory" (SCFT) description of the nanocomposite system. In this approximation, the Hamiltonian is assumed to be described by a single configuration of ω_+ at equilibrium, i.e., the functional derivative $\delta\mathcal{H}/\delta\omega_+ = 0$. ω_+ is relaxed from its initial random configuration toward the equilibrium value ω_+^* by way of a semi-implicit Seidel scheme (SIS), which has resolution and stability improvements over a typical explicit Euler scheme.[35] The SIS scheme is based upon an expansion of the polymer density operators using the random phase approximation to linear order in ω_+, and then subtracting and adding the linear response at the future and current iteration, respectively,

$$\frac{\omega_+^{n+1} - \omega_+^n}{\Delta t} = -g*\omega_+^{n+1} - \frac{\partial\mathcal{H}}{\partial\omega_+} + g*\omega_+^n \quad (7)$$

The $*$ operator in eq 7 represents a convolution of g and ω_+, which is efficiently implemented in Fourier space as a multiplication. The kernel g is given as

$$g(k) = \phi_b F_D(k^2) + \phi_m \alpha F_D(\alpha k^2) \quad (8)$$

where F_D is the Debye function. To aid with convergence, we enforce a requirement that the spatial average of $\omega_+(r) = 0$ by setting $\omega_+(k = 0) \equiv 0$. The time step $\Delta t = 0.5$.

Additional details on the numerical methods employed to solve the field theory are available in a recent publication[36] and a monograph by Fredrickson.[34] The SCFT calculations used the Compute Unified Device Architecture (CUDA) and were performed on NVIDIA Tesla GPUs (M2070-Q) to reduce computation time.

Obtaining Chain Conformation from SCFT. To better compare the SCFT with neutron scattering data, we calculate the scaling of the mean squared end-to-end distance of a brush chain for the system described above, in a manner similar to Schmid[37] and Meth.[38] The probability of a polymer chain starting at position $\mathbf{r}$ and ending at $\mathbf{r}'$ after N steps is given by the Green's function $G(\mathbf{r},\mathbf{r}';N)$, which satisfies a modified diffusion equation,

$$\left[\frac{\partial}{\partial s} - \nabla^2 + i\omega_+^*(\mathbf{r})\right] G(\mathbf{r}, \mathbf{r}'; N) = \delta(\mathbf{r}' - \mathbf{r})\delta(N) \quad (9)$$

where $\omega_+^*(\mathbf{r})$ is the equilibrated auxiliary field, i.e., the saddle-point or mean field configuration. In eq 9, the delta functions enforce the boundary conditions that the chain begins at position $\mathbf{r}$ and that $G(\mathbf{r},\mathbf{r}';N) = 0$ for $N < 0$. The mean squared end-to-end distance of a brush chain anchored at position $\mathbf{R}_0$ is given by

$$\langle {R_{0N}}^2 \rangle = \frac{\int \mathrm{d}\mathbf{R}_N\, (R_0 - R_N)^2 G(\mathbf{R}_0, \mathbf{R}_N; N)}{\int \mathrm{d}\mathbf{R}_N\, G(\mathbf{R}_0, \mathbf{R}_N; N)} \quad (10)$$

In a similar fashion, the mean squared end-to-end distance between the anchored chain end and any segment n can be calculated as

$$\langle {R_{0n}}^2 \rangle = \frac{\iint \mathrm{d}\mathbf{R}_n\, \mathrm{d}\mathbf{R}_N\, (R_0 - R_n)^2 G(\mathbf{R}_0, \mathbf{R}_n; n) G(\mathbf{R}_n, \mathbf{R}_N; N - n)}{\int \mathrm{d}\mathbf{R}_N\, G(\mathbf{R}_0, \mathbf{R}_N; N)} \quad (11)$$

and the mean squared end-to-end distance between a segment n and the free end of the chain as

$$\langle {R_{nN}}^2 \rangle = \frac{\iint \mathrm{d}\mathbf{R}_n\, \mathrm{d}\mathbf{R}_N\, (R_n - R_N)^2 G(\mathbf{R}_0, \mathbf{R}_n; n) G(\mathbf{R}_n, \mathbf{R}_N; N - n)}{\int \mathrm{d}\mathbf{R}_N\, G(\mathbf{R}_0, \mathbf{R}_N; N)} \quad (12)$$

Equation 11 can be interpreted as the mean squared distance between the anchor point, $\mathbf{R}_0$ and segment n for a chain that begins at $\mathbf{R}_0$ and ends at $\mathbf{R}_N$ after N steps. Similarly, eq 12 represents the mean squared distance between segment n and the free end of the chain $\mathbf{R}_N$ subject to the condition that the chain is anchored at a position $\mathbf{R}_0$. Note that this procedure is a highly computationally intensive problem, as it requires that eq

dx.doi.org/10.1021/ma401975a | Macromolecules 2013, 46, 9341−9348

9 be solved at each point $\mathbf{R}_0$ and $\mathbf{R}_n$ to obtain the necessary Green's functions.

EXPERIMENTAL METHODS

Preparation of Nanocomposites. The synthesis of the Fe_3O_4 nanospheres was previously detailed.[39,40] Hydrogenated poly(methyl methacrylate) (hPMMA) was grafted from the nanosphere surface using surface-initiated atom transfer radical polymerization (ATRP). The resulting polymer brushes had a polydispersity index between 1.1 and 1.2.[17,39] Deuterated PMMA matrix polymers with molecular weight M_n = 29 000 g/mol (M_w/M_n < 1.05) and 88 000 g/mol (M_w/M_n = 1.2) were obtained from Polymer Source, Inc. (Montréal, Canada) and used as received. Bulk nanocomposite pellets for small-angle neutron scattering (SANS) were prepared by combining 50 mg of iron oxide nanospheres with 300 mg of deuterated poly(methyl methacrylate) (dPMMA) in toluene, and stirring the solution for approximately 24 h. After allowing the nanoparticles to dissolve, the solution was poured into PDMS molds and the toluene allowed to slowly evaporate over the course of 24 h. Table 1 contains the parameters for all nanocomposites studied. The grafting density σ was measured previously by Xu et al.[39]

Table 1. Parameters for Fe_3O_4 Nanocomposites[a]

sample ID	N	P	$\alpha = P/N$	σ [nm^{-2}]	σ^*
*Fe_3O_4-4K	39	813	21	0.73	2.38
*Fe_3O_4-9K	90	813	9	0.73	3.62
*Fe_3O_4-13K	133	813	6	0.73	4.40
Fe_3O_4-27K$_1$	274	268	1	0.73	6.31
Fe_3O_4-27K$_2$	274	813	3	0.73	6.31
Fe_3O_4-35K	357	813	2	0.73	7.21

[a]The asterisk denotes nanocomposites where nanoparticles aggregated.

Small-Angle Neutron Scattering (SANS) Measurements. SANS was performed on the NG3 30 m SANS instrument at the National Institute for Standards and Technology, Center for Neutron Research (NCNR). Three sample-to-detector distances of 1, 4, and 13 m were used to measure the scattered neutron intensity, $d\Sigma(q)/d\Omega$, as a function of scattering variable $q = (4\pi/\lambda)\sin(\theta/2)$, where θ is the scattering angle and λ is the neutron wavelength (6 Å at 1 and 4 m, 8.4 Å at 13 m).

SANS Analysis: The Core–Shell–Chain Model. The SANS data were analyzed using a core–shell–chain model, where the core represents scattering from the inorganic nanoparticle, the shell represents highly stretched chains in the CPB regime, and the chain portion is due to scattering from the polymer chains in the SDPB regime with an excluded volume parameter ν. In other words, this model makes no assumption that the grafted chains adopt Gaussian conformations, and thus, is a more flexible model for determining brush conformation in solution, or homopolymer melts with favorable Flory–Huggins parameters, χ. The scattering intensity is given by the sum of four scattering factors. $F_A(q)$ is the form factor amplitude of a core–shell nanoparticle. For the spherical Fe_3O_4 nanoparticles, $F_A(q)$ is given by

$$F_A(q) = \left[(\rho_{core} - \rho_{shell})V_{core}\frac{3j_1(qr_{core})}{qr_{core}} + (\rho_{shell} - \rho_{matrix})(V_{shell} + V_{core})\frac{3j_1[q(r_{core} + r_{shell})]}{q(r_{core} + r_{shell})}\right] \quad (13)$$

where j_1 is a spherical Bessel function, r_{core} is the nanoparticle core radius, r_{shell} is the shell thickness, and ρ_i is the scattering length density (SLD) of component i. V_{core} and V_{shell} are the volumes of the core and shell regions, respectively.

The amplitude of correlations between the core–shell particle and grafted polymer chains are given by $F_A(q)F_B(q)$, where

$$F_B(q) = \frac{1 - \exp[-q^2R_g{}^2]}{q^2R_g{}^2} \quad (14)$$

and the radius of gyration squared,

$$R_g{}^2 = \frac{N^{2\nu}a^2}{(2\nu + 1)(2\nu + 2)} \quad (15)$$

Interchain and intrachain correlations are given by $F_B(q)E_A{}^2(q)F_B(q)$ and $P_B(q)$, respectively, where $E_A(q) = j_0[q(r_{core} + r_{shell})]$ is a spherical Bessel function and

$$P_B(q) = 2\int_0^1 dx\,(1 - x)\exp\left[-\frac{q^2a^2}{6}N^{2\nu}x^{2\nu}\right] \quad (16)$$

Hammouda[41] performed the integration of eq 16 to obtain

$$P_B(q) = \frac{1}{\nu U^{1/2\nu}}\gamma\left(\frac{1}{2\nu}, U\right) - \frac{1}{\nu U^{1/\nu}}\gamma\left(\frac{1}{\nu}, U\right) \quad (17)$$

In eq 17, $\gamma(d,U)$ is the lower incomplete γ function with the form

$$\gamma(d, U) = \int_0^U dt\ e^{-t}t^{d-1} \quad (18)$$

and the variable $U = q^2a^2N^{2\nu}/6$. With these correlation terms defined, the scattering cross section (in units of cm^{-1}) for nanoparticles at a number density N_P/V with N_g grafted polymer chains per particle is

$$\frac{d\Sigma(q)}{d\Omega} = \frac{N_P}{V}[F_A(q)^2 + N_gV_BF_A(q)F_B(q) + N_g(N_g - 1)V_B{}^2F_B(q)E_A{}^2(q)F_B(q) + N_gV_B{}^2P_B(q)]S_I(q) \quad (19)$$

For well-dispersed particles, we approximate the interparticle structure factor term as $S_I(q) \approx 1$. The polymer chain volume $V_B = N/\rho_0$. The excluded volume parameter ν yields information regarding the brush chain conformation. For $\nu \approx {}^3/_5$, the conformation is described by a self-avoiding random walk, whereas for $\nu = {}^1/_3$ and $\nu = 1$, the conformation is described by a self-attracting walk or a thin rigid rod, respectively. Note, however, that setting $\nu = 1$ in eq 16 does not reproduce the correct rigid rod limit, and that the $F_B(q)E_A{}^2(q)F_B(q)$ term is approximate. For $\nu = {}^1/_2$, the chain conformation is that of a pure random walk, and if $r_{shell} \to 0$, eq 19 reduces to Pedersen's model for grafted Gaussian chains.[28] For each set of SANS data, ν, R_g and r_{shell} were determined from nonlinear least-squares fitting. r_{core} was measured previously by Xu et al.[39] using transmission electron microscopy (TEM). Recall that $r_c = r_{core} + r_{shell}$ (*cf.*, eq 1). The scattering length densities of the nanoparticles, brush, and matrix are summarized in Table 2.

Table 2. Scattering Length Densities for Polymer Nanocomposite Components

material	scattering length density, Å^{-2}	ref
Fe_3O_4	6.97×10^{-6}	42
deuterated PMMA	6.88×10^{-6}	43
hydrogenated PMMA	1.05×10^{-6}	43

RESULTS AND DISCUSSION

SCFT Chain Conformation. The effect of $\alpha = P/N$ on the interaction free energy between pairs of nanospheres has been studied previously by Xu et al.,[24] by Kim and Matsen,[21] and, most recently, by Trombly and Ganesan[23] using SCFT in the context of predicting nanosphere dispersion. Here, only the structure of the brush chains is considered. Shown in Figure 2 are brush density profiles for nanocomposite systems analogous to the Fe_3O_4-27K$_1$ system (σ^* = 6.31, red), and one at a lower reduced grafting density σ^* = 1.00 (black). The bottom axis

dx.doi.org/10.1021/ma401975a | Macromolecules 2013, 46, 9341–9348

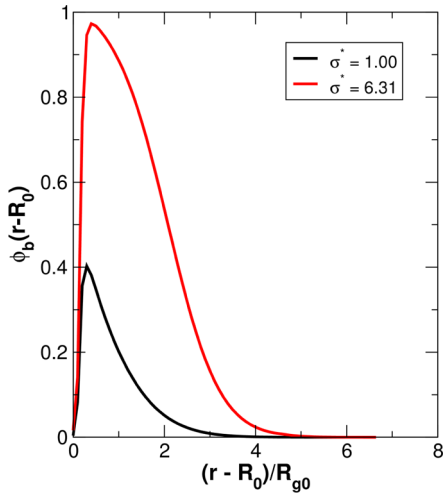

Figure 2. Polymer brush density profiles determined from SCFT calculations corresponding to the Fe_3O_4-27K_1 system (red), and one at a lower grafting density (black). For both systems, $\alpha = P/N = 1$.

represents the distance from the grafting surface of the nanoparticle, $r - R_0$, normalized by the unperturbed radius of gyration of a brush chain, $R_{g0} = a(N/6)^{1/2}$. Note that according to eq 4, $\sigma^* = 1.00$ corresponds to roughly 0.1 chains/nm^2. As σ^* increases, the brush density increases due to the larger number of brush chains that are attached to the nanoparticle surface. The effect of grafting density on the brush density profiles can be quantified through the brush height, defined as the position at which the brush density drops to one-half of its initial value, $\phi_b(h_b) = 1/2\phi_b(0)$. The height of the brush, h_b, increases from approximately 1.12 R_{g0} to 2.36 R_{g0} as σ^* increases from 1.00 to 6.31. This effect is due to the fact that the chains are increasingly stretched due to steric interactions between the brush chains. Notice that for $\sigma^* = 6.31$, the brush chains do not appear to be significantly stretched. If σ^* is increased to 13.48 (not shown), the brush density profile becomes more step-like, which is indicative of a higher degree of stretching. In Figure 3, the brush density profiles are shown for Fe_3O_4-27K_1 (black) and Fe_3O_4-27K_2 (red). For these two

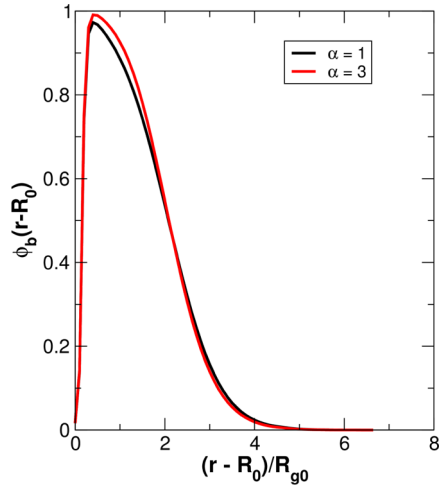

Figure 3. Polymer brush density profiles determined from SCFT calculations corresponding to the Fe_3O_4-27K_1 nanocomposite (black), for which $\alpha = 1$, and Fe_3O_4-27K_2 (red), for which $\alpha = 3$. For both systems, $\sigma^* = 6.31$.

nanocomposites, only the molecular weight of the matrix polymer varies. Thus, the ratio of the degree of polymerization of the matrix to that of the brush, $\alpha = P/N$, varies from 1 for Fe_3O_4-27K_1 to approximately 3 for Fe_3O_4-27K_2. Only subtle differences are observed in the density profiles for the two nanocomposite systems, such as a slight enrichment of the polymer brush near the nanoparticle surface for $\alpha \approx 3$. These results are in qualitative agreement with similar calculations for other nanocomposite systems.[5,21,23,30] Hence, no significant differences in the brush chain conformation between the two nanocomposites are expected to be observed in SANS measurements.

Chain stretching in the brush can be quantified using the mathematical formalism of eqs 9−12. In particular, the excluded volume parameter ν can be obtained from the scaled end-to-end distance, R_{ee}/R_{g0} as

$$\nu = \frac{1}{2}\left[\frac{\log(N\tilde{R}_{ee}^{\,2}/2d)}{\log n}\right] \tag{20}$$

where $\tilde{R}_{ee}^{\,2} = (R_{ee}/R_{g0})^2$, d is the dimensionality of the calculation space, and n is an arbitrary position along the polymer contour, $0 \le n \le N$. ν is representative of chain crowding, as large values of ν imply a more strongly stretched polymer chain. The excluded volume parameters for $R_{ee} = R_{0n}$ and $R_{ee} = R_{nN}$ are shown in Figure 4. Note that the black line in

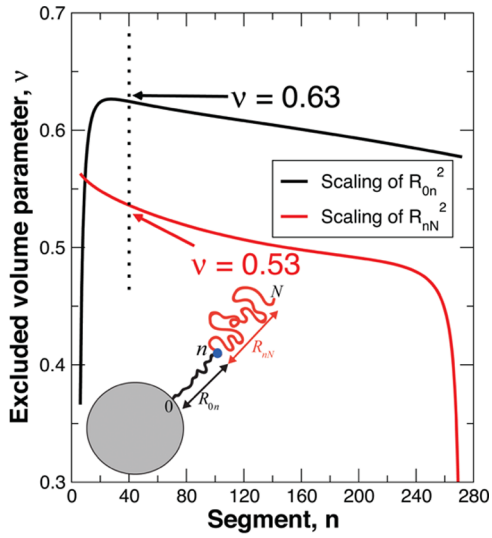

Figure 4. Excluded volume parameter, ν, determined from SCFT calculations. The black curve corresponds to the scaling of the end-to-end distance from the anchor point to the segment at position n (R_{0n}), whereas the red curve corresponds to the scaling of the end-to-end distance from position n to the free end of the chain (R_{nN}). For example, for $n = 40$, $\langle R_{0n}^{\,2}\rangle^{1/2} \sim n^{0.63}$ and $\langle R_{nN}^{\,2}\rangle^{1/2} \sim (N - n)^{0.53}$, as indicated by the dotted line. The parameters $\sigma^* = 6.31$ and $\alpha = 1$. R_{0n} and R_{nN} are depicted schematically in the illustration.

Figure 4 represents the scaling of the root mean-squared end-to-end distance between the anchor point at the nanoparticle surface, and segment n, whereas the red line represents the scaling of the root mean-squared end-to-end distance between segment n and the free end of the chain, as depicted schematically in Figure 4. For example, if $n = 40$, $\langle R_{0n}^{\,2}\rangle^{1/2} \sim n^{0.63}$ and $\langle R_{nN}^{\,2}\rangle^{1/2} \sim (N - n)^{0.53}$, as indicated by the dotted line in Figure 4. Note that the maximum value of ν in the scaling relationship of $\langle R_{0n}^{\,2}\rangle^{1/2}$ is slightly larger than 0.6, whereas the

dx.doi.org/10.1021/ma401975a | Macromolecules 2013, 46, 9341−9348

value of ν in the scaling relationship of $\langle R_{nN}^2\rangle^{1/2}$ decreases from approximately 0.57 to 0.50 over the range of n shown in Figure 4. These results represent a weaker degree of stretching of the brush near the nanoparticle surface than is expected from the scaling analysis of Ohno et al.[17] and Dukes et al.[18] If σ^* is increased beyond 6.31, the chains become more stretched as indicated by a larger maximum value of ν. However, for the parameters relevant to the experimental system, SCFT predicts $\nu \approx 0.6$ in the CPB regime and $\nu \approx 0.50$ in the SDPB regime.

The profiles from SCFT exhibit a small degree of chain stretching near the nanoparticle surface, and a scaling of the remainder of the chain $\langle R_{nN}^2\rangle^{1/2} \sim N^{\nu}$ where $0.50 \leq \nu \leq 0.55$. A recent study by Frischknecht et al.[5] that compares classical DFT calculations to SCFT demonstrates that at the same reduced grafting densities, the density profiles obtained from SCFT show a lesser degree of stretching as compared to DFT. However, if the reduced grafting density of the DFT calculations decreases, or correspondingly, the grafting density of the SCFT calculations increases, the two profiles are in excellent agreement. This difference may be due to certain assumptions in the SCFT or a lack of parameters, such as the assumption of a very large molecular weight polymer, lack of an explicit chain length variable, or a poor description of the polymer chain near the nanoparticle surface, where numerical divergences in the auxiliary field have been shown to occur.[33] Thus, the SCFT results presented in Figures 2−4 likely underpredict the degree of stretching in the brush, as will be shown in the following section describing the neutron scattering measurements Additional work is required to better connect experimental values of σ with relevant values of σ^* in the SCFT to more accurately model the brush density profile and brush chain conformation.

SANS of Iron Oxide Nanocomposites. In contrast to the SCFT results above, small-angle neutron scattering measurements indicate the presence of both a CPB and SDPB region in the hPMMA brush that is grafted to 2.5 nm iron oxide nanoparticles. SANS scattering intensities for the Fe_3O_4-4K, Fe_3O_4-9K, and Fe_3O_4-13K nanocomposites are shown in Figure 5 as a function of scattering variable q. The nanoparticles comprise 14%, by mass, of the nanocomposite. The power law observed as $q \to 0$ is indicative of large nanoparticle aggregates. A peak in the scattering intensity is observed near $q = 0.09$ Å^{-1}, corresponding to a length scale of approximately 7 nm. We attribute this peak to an interparticle structure factor between aggregated nanoparticles. Note that aggregation is observed for $\alpha = P/N \geq 6$, which is in qualitative agreement with previous studies by others.[2,3,39] The scanning electron microscope (SEM) image in Figure 6 corroborates the SANS analysis,

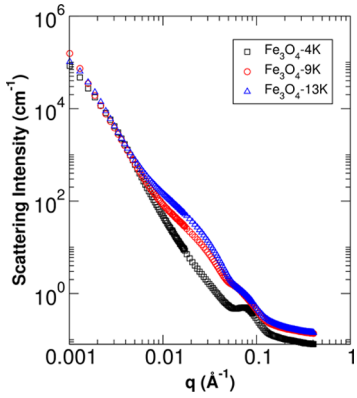

Figure 5. Scattering intensities for Fe_3O_4-4K (black), Fe_3O_4-9K (red), and Fe_3O_4-13K (blue) showing aggregation of nanoparticles due to depletion-attractions, since $\alpha \geq 6$. Error bars are smaller than the plotting symbols.

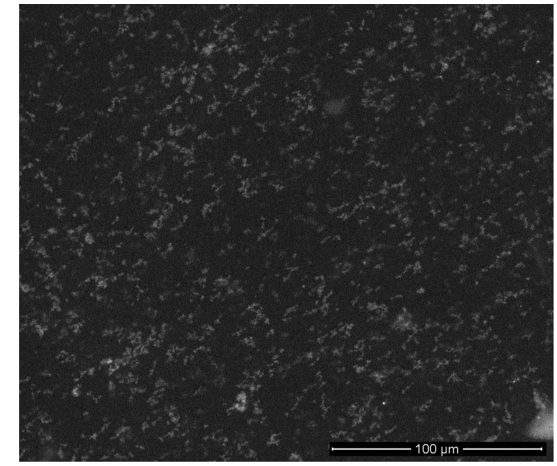

Figure 6. Scanning electron microscopy image of the Fe_3O_4-4K nanocomposite. The bright regions correspond to nanoparticle aggregates.

and shows large aggregates of nanoparticles. Because of the scattering from nanoparticle aggregates in these systems, fitting the SANS intensity to determine the hPMMA brush conformation is not possible.

Small-angle scattering intensities for the Fe_3O_4-27K systems are shown in Figure 7, along with fits using the core−shell−

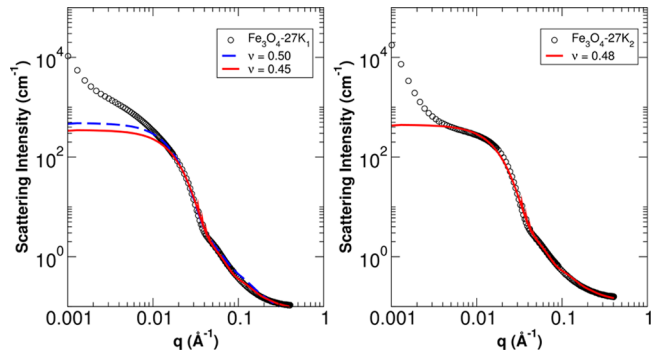

Figure 7. Scattering intensities for iron oxide nanoparticles with 27 kg/mol hPMMA brushes. (Left) SANS from Fe_3O_4-27K$_1$. (Right) SANS from Fe_3O_4-27K$_2$. The red lines are best fits using the core−shell−chain model above. For comparison, the blue line for the Fe_3O_4-27K$_1$ system is the best fit holding $\nu = 0.50$ fixed. Error bars are smaller than the plotting symbols.

chain model presented in a previous section. The scattering intensity is characterized by a tail at small values of q ($q < 0.002$ Å^{-1}), followed by a Guinier-like region for intermediate values of q, and finally a tail for $q > 0.03$ Å^{-1} due to scattering from the hPMMA chains. Note that because of the low q tail, a Guinier region where the scattering intensity $I(q) \sim q^0$ is not observed. In the core−shell−chain fits, the scattering length density (SLD) of the shell was fixed to the value for hPMMA, and yielded a consistent value of the shell thickness for both Fe_3O_4-27K$_1$ and Fe_3O_4-27K$_2$. The structure obtained from a best fit of

dx.doi.org/10.1021/ma401975a | Macromolecules 2013, 46, 9341−9348

the scattered intensity is a spherical iron oxide core with radius r_{core} = 2.5 nm surrounded by an hPMMA shell with an approximate thickness 4 nm. The chains outside of the shell adopt a radius of gyration $R_g \sim N^{\nu}$ with R_g = 5.406 ± 0.008 nm and ν = 0.4520 ± 0.0003 for Fe_3O_4-27K$_1$, R_g = 5.537 ± 0.003 nm and ν = 0.4854 ± 0.0004 for Fe_3O_4-27K$_2$. Note that the values of ν are consistent with those obtained for $\langle R_{nN}^2 \rangle^{1/2}$ from SCFT (*cf.*, Figure 4). The SANS intensity for the Fe_3O_4-35K system is shown in Figure 8. The best fit, using the core–shell–chain model, yields similar results to the Fe_3O_4-27K systems. In particular, a shell with thickness 3.9 nm is observed, with the chain size scaling as $N^{0.50}$ in the SDPB region. Recall that eq 1 predicts that the CPB region extends approximately 5.6 to 7.0 nm from the nanoparticle center. Thus, the measured values of r_{shell} yield $r_c = r_{core} + r_{shell} \approx 6.4$ nm, which is in excellent agreement with the scaling predictions in the literature. Furthermore, eq 1 predicts that the shell thickness is independent of the degree of polymerization of the brush, N. For this reason, r_{shell} is expected to be relatively similar for both the Fe_3O_4-27K and Fe_3O_4-35K nanocomposite systems. In addition, the Gaussian behavior (i.e., ν = 0.5) of the chains in the SDPB region is in excellent agreement with the measurements performed by Choi et al. of polystyrene-grafted silica particles.[19,20]

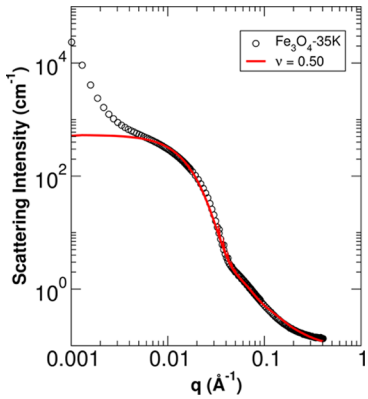

Figure 8. Scattering intensity for Fe_3O_4-35K. Error bars are smaller than the plotting symbols.

The fit parameters for the three nanocomposite systems are summarized in Table 3. The results for the Fe_3O_4-27K$_1$ and Fe_3O_4-27K$_2$ composites demonstrate that the molecular weight of the polymer matrix has little influence on the brush chain conformation, which is good agreement with the SCFT results in Figure 3 and a previous study.[30] Note that while SCFT does predict a very subtle compression of the brush as α increases from 1 to 3, this change in polymer density is too small to resolve in our data. Specifically, the differences between r_{shell} and R_g for the Fe_3O_4-27K$_1$ and Fe_3O_4-27K$_2$ composites are both on the order of 0.3 nm, implying that within the accuracy of our measurements, we cannot resolve the small compression predicted by SCFT. As expected, R_g is larger for the Fe_3O_4-35K system due to the larger molecular weight of the brush chains. In agreement with eq 1, r_{shell} remains relatively constant as the molecular weight of the brush varies. To the best of our knowledge, these data represent the first direct measurement of the CPB and SDPB regions of highly grafted nanoparticles.

Table 3. Core–Shell–Chain Model Parameters Determined from Fits to SANS Intensity[a]

sample ID	r_{shell} [nm]	R_g [nm]	ν
Fe_3O_4-27K$_1$	3.930 ± 0.008	5.406 ± 0.008	0.4520 ± 0.0003
Fe_3O_4-27K$_2$	4.290 ± 0.006	5.537 ± 0.003	0.4854 ± 0.0004
Fe_3O_4-35K	3.902 ± 0.010	6.239 ± 0.005	0.4997 ± 0.0004

[a]For all fits, the nanoparticle radius r_{core} was fixed at 2.5 nm. Statistical errors correspond to 1 standard deviation.

SUMMARY

In summary, we have conducted small-angle neutron scattering (SANS) measurements of poly(methyl methacrylate)-functionalized (PMMA) Fe_3O_4 nanospheres within a deuterated PMMA matrix. Unlike previous measurements that relied on inferring the structure of the polymer brush using dynamic light scattering (DLS)[17,18] or electron microscopy,[20,19] the SANS measurements are able to *directly* probe the concentrated polymer brush (CPB) and semidilute polymer brush (SDPB) regions of the grafted polymer chains. The results of these measurements are in good agreement with the scaling arguments presented by Ohno et al.,[17] the DLS results from both Ohno et al. and Dukes et al.,[18] as well as measurements by electron microscopy by Choi et al.[20,19] Self-consistent field theory (SCFT) calculations underestimate chain stretching in the CPB region of the brush, although they give an approximate picture of the chain conformation in our nanocomposite systems. On the other hand, SCFT accurately predicts the polymer chain conformation in the SDPB region. An open problem going forward is determing how best to connect experimental grafting densities with reduced grafting densities in SCFT to obtain accurate brush density profiles and more accurate measures of brush chain conformation.

We have extended the small-angle scattering models in the literature[28,29] to describe scattering from a highly grafted nanoparticle with grafted chains that are not assumed to obey Gaussian statistics. In this model, the conformation of the brush chains away from the nanoparticle surface is described by an excluded volume parameter ν. For an ideal chain $\nu = {}^1/_2$, whereas $\nu = {}^1/_3$ and $\nu = {}^3/_5$ for collapsed and swollen coils, respectively. Fits to our SANS data yield values of ν near ${}^1/_2$, indicating that the brush chains behave as ideal random walks in the SDPB region of the brush when in a homopolymer melt. Going forward, the SANS model presented in this article can be extended and applied to more complex systems, such as nonspherical nanoparticles, polymer-grafted nanoparticles in good or poor solvents, or grafted polyelectrolyte brushes.

AUTHOR INFORMATION

Corresponding Author

*E-mail: (M.J.A.H.)michael.hore@nist.gov.

Notes

The authors declare no competing financial interest.

ACKNOWLEDGMENTS

The identification of commercial products or experimental methods does not imply endorsement by the National Institute of Standards and Technology nor does it imply that these are the best for the purpose. This work utilized neutron scattering facilities supported in part by the National Science Foundation (NSF) under Agreement No. DMR-0944772. M.J.A.H. acknowledges support from a National Research Council (NRC) postdoctoral associateship at the NIST Center for

Neutron Research (NCNR). R.J.C. acknowledges support from NSF Polymer DMR-0907493 and CEMRI DMR-1120901 Programs. Tim Mori (NCSU Libraries) is acknowledged for providing access to NVIDIA Tesla GPUs. We thank Amalie Frischknecht (Sandia), August Bosse (ExxonMobil), Jeff Meth (DuPont), and Jihoon Choi (Penn) for helpful discussions.

REFERENCES

(1) Huynh, W. U.; Dittmer, J. J.; Alivisatos, A. P. *Science* **2002**, *295*, 2425−2427.
(2) Green, P. F. *Soft Matter* **2011**, *7*, 7914−7926.
(3) Kumar, S. K.; Jouault, N.; Benicewicz, B.; Neely, T. *Macromolecules* **2013**, *46*, 3199−3214.
(4) Hore, M. J. A.; Frischknecht, A. L.; Composto, R. J. *ACS Macro Lett* **2012**, *1*, 115−121.
(5) Frischknecht, A. L.; Hore, M. J. A.; Ford, J.; Composto, R. J. *Macromolecules* **2013**, *46*, 2856−2869.
(6) Frischknecht, A. L. *J. Chem. Phys.* **2008**, *128*, 224902.
(7) Jiao, Y.; Akcora, P. *Macromolecules* **2012**, *45*, 3463−3470.
(8) Gam, S.; Meth, J. S.; Zane, S. G.; Chi, W.; Wood, B. A.; Seitz, M. E.; Winey, K. I.; Clarke, N.; Composto, R. J. *Macromolecules* **2011**, *44*, 3494−3501.
(9) Gam, S.; Meth, J. S.; Zane, S. G.; Chi, C.; Wood, B. A.; Winey, K. I.; Clarke, N.; Composto, R. J. *Soft Matter* **2012**, *8*, 6512−6520.
(10) Choi, J.; Hore, M. J. A.; Meth, J. S.; Clarke, N.; Winey, K. I.; Composto, R. J. *ACS Macro Lett* **2013**, *2*, 485−490.
(11) Alexander, S. *J. Phys. (Paris)* **1977**, *38*, 983−987.
(12) de Gennes, P. G. *J. Phys. (Paris)* **1976**, *37*, 1445−1452.
(13) Daoud, M.; Cotton, J. P. *J. Phys. (Paris)* **1982**, *43*, 531−538.
(14) Zhulina, E. B.; Birshtein, T. M.; Borisov, O. V. *Eur. Phys. J. E* **2006**, *20*, 243−256.
(15) Laradji, M. *Europhys. Lett.* **2002**, *60*, 594−600.
(16) Laradji, M. *J. Chem. Phys.* **2004**, *121*, 1591.
(17) Ohno, K.; Morinaga, T.; Takeno, S.; Tsujii, Y.; Fukuda, T. *Macromolecules* **2007**, *40*, 9143−9150.
(18) Dukes, D.; Li, Y.; Lewis, S.; Benicewicz, B.; Schadler, L.; Kumar, S. K. *Macromolecules* **2010**, *43*, 1564−1570.
(19) Choi, J.; Dong, H.; Matyjaszewski, K.; Bockstaller, M. R. *J. Am. Chem. Soc.* **2010**, *132*, 12537−12539.
(20) Choi, J.; Hui, C. M.; Schmitt, M.; Pietrasik, J.; Margel, S.; Matyjaszewski, K.; Bockstaller, M. R. *Langmuir* **2013**, *29*, 6452−6459.
(21) Kim, J. U.; Matsen, M. W. *Macromolecules* **2008**, *41*, 4435−4443.
(22) Dan, N.; Tirrell, M. *Macromolecules* **1992**, *25*, 2890−2895.
(23) Trombly, D. M.; Ganesan, V. *J. Chem. Phys.* **2010**, *133*, 154904.
(24) Xu, J.; Qiu, F.; Zhang, H.; Yang, Y. *J. Polym. Sci. B: Polym. Phys.* **2006**, *44*, 2811−2820.
(25) Chevigny, C.; Gigmes, D.; Bertin, D.; Jestin, J.; Boué, F. *Soft Matter* **2009**, *5*, 3741−3753.
(26) Chevigny, C.; Jestin, J.; Gigmes, D.; Schweins, R.; Di-Cola, E.; Dalmas, F.; Bertin, D.; Boué, F. *Macromolecules* **2010**, *43*, 4833−4837.
(27) Chevigny, C.; Dalmas, F.; Di Cola, E.; Gigmes, D.; Bertin, D.; Boué, F.; Jestin, J. *Macromolecules* **2011**, *44*, 122−133.
(28) Pedersen, J. S.; Gerstenberg, M. C. *Macromolecules* **1996**, *29*, 1363−1365.
(29) Pedersen, J. S. *Adv. Colloid Interface Sci.* **1997**, *70*, 171−210.
(30) Vogiatzis, G. G.; Theodorou, D. N. *Macromolecules* **2013**, *46*, 4670−4683.
(31) Robbes, A. S.; Cousin, F.; Meneau, F.; Dalmas, F.; Schweins, R.; Gigmes, D.; Jestina, J. *Macromolecules* **2012**, *45*, 9220−9231.
(32) Robbes, A. S.; Cousin, F.; Meneau, F.; Chevigny, C.; Gigmes, D.; Fresnais, J.; Schweins, R.; Jestin, J. *Soft Matter* **2012**, *8*, 3407−3418.
(33) Chantawansri, T. L.; Hur, S.-M.; García-Cervera, C. J.; Ceniceros, H. D.; Fredrickson, G. H. *J. Chem. Phys.* **2011**, *134*, 244905.
(34) Fredrickson, G. H. *The Equilibrium Theory of Inhomogeneous Polymers*; Oxford University Press: New York, 2006.
(35) Ceniceros, H. D.; Fredrickson, G. H. *Multiscale Model. Simul.* **2004**, *3*, 452.
(36) Hore, M. J. A.; Composto, R. J. *Macromolecules* **2012**, *45*, 6078−6086.
(37) Schmid, F.; Müller, M. *Macromolecules* **1995**, *28*, 8639−8645.
(38) Meth, J. S.; Lustig, S. R. *Polymer* **2010**, *51*, 4259−4266.
(39) Xu, C.; Ohno, K.; Ladmiral, V.; Composto, R. J. *Polymer* **2008**, *49*, 3568−3577.
(40) Ohno, K.; Morinaga, T.; Koh, K.; Tsujii, Y.; Fukuda, T. *Macromolecules* **2005**, *38*, 2137−2142.
(41) Hammouda, B. *Adv. Polym. Sci.* **1993**, *106*, 87−133.
(42) Krycka, K. L.; Borchers, J. A.; Booth, R. A.; Hogg, C. R.; Ijiri, Y.; Chen, W. C.; Watson, S. M.; Laver, M.; Gentile, T. R.; Harris, S.; Dedon, L. R.; Rhyne, J. J.; Majetich, S. A. *J. Appl. Phys.* **2010**, *107*, 09B525.
(43) Zeroni, I.; Lodge, T. P. *Macromolecules* **2008**, *41*, 1050−1052.